



HAL
open science

Improved mitochondrial coupling as a response to high mass-specific metabolic rate in extremely small mammals

Mélanie Boël, Caroline Romestaing, Claude H. B. Duchamp, Frederic Veyrunes, Sabrina Renaud, Damien Roussel, Yann Voituron

► To cite this version:

Mélanie Boël, Caroline Romestaing, Claude H. B. Duchamp, Frederic Veyrunes, Sabrina Renaud, et al.. Improved mitochondrial coupling as a response to high mass-specific metabolic rate in extremely small mammals. *Journal of Experimental Biology*, 2020, 223 (5), pp.jeb215558. 10.1242/jeb.215558 . hal-02506463

HAL Id: hal-02506463

<https://univ-lyon1.hal.science/hal-02506463v1>

Submitted on 4 Jun 2021

HAL is a multi-disciplinary open access archive for the deposit and dissemination of scientific research documents, whether they are published or not. The documents may come from teaching and research institutions in France or abroad, or from public or private research centers.

L'archive ouverte pluridisciplinaire **HAL**, est destinée au dépôt et à la diffusion de documents scientifiques de niveau recherche, publiés ou non, émanant des établissements d'enseignement et de recherche français ou étrangers, des laboratoires publics ou privés.

RESEARCH ARTICLE

Improved mitochondrial coupling as a response to high mass-specific metabolic rate in extremely small mammals

Mélanie Boël^{1,†}, Caroline Romestaing¹, Claude Duchamp¹, Frédéric Veyrunes², Sabrina Renaud³, Damien Roussel^{1,*} and Yann Voituron^{1,*}

ABSTRACT

Mass-specific metabolic rate negatively co-varies with body mass from the whole-animal to the mitochondrial levels. Mitochondria are the mainly consumers of oxygen inspired by mammals to generate ATP or compensate for energetic losses dissipated as the form of heat (proton leak) during oxidative phosphorylation. Consequently, ATP synthesis and proton leak compete for the same electrochemical gradient. Because proton leak co-varies negatively with body mass, it is unknown whether extremely small mammals further decouple their mitochondria to maintain their body temperature or whether they implement metabolic innovations to ensure cellular homeostasis. The present study investigated the impact of body mass variation on cellular and mitochondrial functioning in small mammals, comparing two extremely small African pygmy mice (*Mus mattheyi*, ~5 g, and *Mus minutoides*, ~7 g) with the larger house mouse (*Mus musculus*, ~22 g). Oxygen consumption rates were measured from the animal to the mitochondrial levels. We also measured mitochondrial ATP synthesis in order to appreciate the mitochondrial efficiency (ATP/O). At the whole-animal scale, mass- and surface-specific metabolic rates co-varied negatively with body mass, whereas this was not necessarily the case at the cellular and mitochondrial levels. *Mus mattheyi* had generally the lowest cellular and mitochondrial fluxes, depending on the tissue considered (liver or skeletal muscle), as well as having more-efficient muscle mitochondria than the other two species. *Mus mattheyi* presents metabolic innovations to ensure its homeostasis, by generating more ATP per oxygen consumed.

KEY WORDS: *Mus*, Oxidative phosphorylation, Allometry, Mitochondrial efficiency, Liver, Muscles

INTRODUCTION

Body size is well known to impact biological structures and processes from cellular metabolism to population dynamics (Peters, 1983; McMahon and Bonner, 1983; Schmidt-Nielsen, 1984). Therefore, considerable effort in documenting patterns in size distribution and evolutionary size change among organisms has been expended (Brown, 1995; Boback and Guyer, 2003). The

resulting body size frequency distribution obtained in endotherms is strongly right-skewed, with modal classes at 13 and 21 g for birds and mammals, respectively (Blackburn and Gaston, 1994; Gardezi and da Silva, 1999). Such skewness shows a limited scope to become significantly smaller than the modal body size. Artificial selection experiments (Roberts, 1966, 1981; Falconer, 1973) provide information about the genetic basis of small size selection, but also emphasize the role of correlated responses in other traits such as reproductive phenology (Hillesheim and Stearns, 1992), thermoregulation (Lynch and Roberts, 1984) and metabolism (Malerba et al., 2018). In endotherms, thermoregulation and metabolism are closely linked because cellular metabolism, in addition to providing energy essential to an organism, also generates heat that determines body temperature. Such a link partly explains why mass-specific metabolic rate co-varies negatively with body mass (BM) according to BM^b , where the scaling exponent b varies among taxa but is generally equal to $-1/4$ (Hayssen and Lacy, 1985; Glazier, 2005). In particular, Pearson (1947, 1948) showed that this relationship is also found for very small species with a smaller scaling exponent than expected ($<-1/4$), and said consequently: ‘A mammal smaller than this would be unable to gather enough food to support its infinitely rapid metabolism and would have to resort to a lowered body temperature or some other fundamental method of conserving energy’. To offset the high energetic cost of endothermy, very small mammals have thus developed various energy-saving strategies, which can include torpor, hibernation and behavioural adaptations (Heldmaier, 1989; Terrien et al., 2011). However, it is questionable whether these adaptations are sufficient and whether there would not be additional metabolic innovations at the cellular level to address this very high energy cost.


In aerobic organisms, oxygen inspired is mainly consumed (90%) within a cell by mitochondria to generate cellular energy (ATP) via the oxidative phosphorylation process (Rolfe and Brown, 1997). Briefly, this bioenergetics process is enabled by the formation of a proton electrochemical gradient across the mitochondrial inner membrane, which is used to synthesize ATP by ATP synthase or to compensate for energy loss inherent to this process, which is mainly due to proton leakage. Proton leak is a major contributor of cellular resting metabolic rate (from 20% in hepatocytes to 50% in resting skeletal muscle) and accounts for up to 20–25% of basal metabolic rate in rats (Rolfe and Brand, 1996, 1997; Rolfe et al., 1999; Divakaruni and Brand, 2011). This energy loss is driven by proton conductance pathways within the inner mitochondrial membrane, which have been found to negatively correlate with body mass (Porter and Brand, 1993; Porter et al., 1996; Brand et al., 2003; Polymeropoulos et al., 2011). This means that smaller species have mitochondria that are more uncoupled with higher leak than larger ones. This characteristic may be of physiological interest in small organisms to produce more heat at rest. However, considering that ATP synthesis and proton leakage compete for the same driving

¹Laboratoire d'Ecologie des Hydrosystèmes Naturels et Anthropisés (UMR CNRS 5023), Université Claude Bernard Lyon 1, Université de Lyon, ENTPE, 69622 Villeurbanne Cedex, France. ²Institut des Sciences de l'Evolution de Montpellier (UMR CNRS 5554), Université Montpellier, IRD, EPHE, 34095 Montpellier, France.

³Laboratoire de Biométrie et Biologie Evolutive (UMR CNRS 5558), Université Claude Bernard Lyon 1, Université de Lyon, 69622 Villeurbanne Cedex, France.

*These authors contributed equally to this work

†Author for correspondence (melanie.boel@univ-lyon1.fr)

 M.B., 0000-0003-4286-6139; C.R., 0000-0002-6877-9626; C.D., 0000-0001-9853-7110; F.V., 0000-0002-1706-9915; S.R., 0000-0002-8730-3113; D.R., 0000-0002-8865-5428; Y.V., 0000-0003-0572-7199

force, the electrochemical gradient protons, very high proton leakage might also compromise cellular ATP homeostasis as well as animal performance by drastically decreasing ATP production. This implies that there is a cost to being leaky, suggesting that extremely small mammals might not be able to compensate for the huge energy wastage induced by proton leak while sustaining life. Consequently, the trade-off between generating ATP to ensure cellular homeostasis and proton leakage, which dissipates energy in the form of heat, suggests that in extremely small mammals, mitochondrial metabolic innovations must be found to fulfil cellular energy needs and ensure homeostasis.

This study aimed to investigate mitochondrial functioning in liver and skeletal muscle of three rodents exhibiting body masses from small (the house mouse *Mus musculus*, ~22 g) to very small (the African pygmy mice *Mus minutoides*, ~7 g, and *Mus mattheyi*, ~5 g; Britton-Davidian et al., 2012). Thus, by comparing whole-animal and cellular oxygen consumption together with mitochondrial oxidative phosphorylation activity and efficiency, i.e. the mitochondrial capacity to synthesize a certain quantity of ATP per oxygen consumed (ATP/O), we questioned whether whole-animal metabolic rates and cellular oxygen consumption, as well as mitochondrial ATP synthesis, follow a common inter-specific allometric relationship across the size range of small mammals or whether mitochondria show metabolic enhancements to ensure homeostasis in extremely small mammals.

MATERIALS AND METHODS

Animals

African pygmy mice [*Mus minutoides* (A Smith 1834), $n=30$, and *Mus mattheyi* Petter 1969, $n=25$] were all male and obtained from the CECEMA (Montpellier University). House mice (*Mus musculus* Linnaeus 1758, $n=24$) were also male and were born in the laboratory (EcoAquatron, Lyon University) from the breeding of specimens collected in the wild (45°49'58.9"N, 5°05'47.8"E). These species were chosen because they belong to the genus *Mus* and are phylogenetically closely related (Veyrunes et al., 2005). All experiments were conducted in accordance with animal care guidelines and were approved by the ethics committees of Lyon and Montpellier University, as well as the Ministère de la Recherche et de l'Enseignement Supérieur.

Energy expenditure during rest or activity

Free-living energy expenditure of pygmy and house mice was measured using a PhenoMaster Indirect Calorimetry System (TSE Systems, Bad Homburg, Germany) equipped for parallel measurements of an empty reference cage and four individual mouse cages. Mice were alone in the cage, with sawdust and cardboard roll as a nest, but could at least see each other through the plastic walls. Air was flowed through the cages at a constant rate of 0.25 l min⁻¹ and a sample flow rate of 0.2 l min⁻¹ was used. Air samples were analysed with a high-speed Siemens Ultramat/Oxymat 6 O₂/CO₂ analyser (TSE Systems) in a measuring range for O₂ between 20.0% and 21.5% and for CO₂ between 0.0% and 1.0%. The analyser was calibrated with air and a gas mixture containing 20.237% O₂ and 0.944% CO₂ (Air Liquide, Paris, France). The O₂/CO₂ composition of the air leaving each cage was analysed for 2 min to ensure sufficient stabilization of the analyser and this was repeated every 10 min for 2–4 successive days. Rates of oxygen consumption and carbon dioxide production were calculated by TSE Systems software, using the reference cage for measurement of oxygen and carbon dioxide inflow. The caloric equivalent for O₂ was determined from the respiratory quotient

using Lusk tables (Lusk, 1924). Metabolic cage measurements were conducted continuously for 55–96 h (2–4 days) to account for acclimation of mice to their cages. Ambient temperature within the cages was about 23°C and photoperiod followed a 12 h:12 h light:dark cycle. Food and water were available *ad libitum* during the whole experiment. As the species are nocturnal, the resting metabolic rate (RMR) was estimated as the average of the 10% of lowest values recorded during the daytime and the active metabolic rate (AMR) by the average of the 10% of highest values monitored during the night-time for each individual. All measurements were recorded at ~23°C, a temperature below the thermoneutrality zone of mice (~28°C for *M. musculus* and above 30°C for the other two species; Hoole et al., 2019; Keijer et al., 2019). Heat loss is strongly dependent on the body surface of animals and the surface area of mammals correlates positively with body mass according to an exponent of 0.67 (Reynolds, 1997). Metabolic rate was initially expressed by body mass of the individual (W g⁻¹); however, in order to consider differences in body surface and heat loss between species, we then calculated the surface-specific metabolic rate, expressing metabolic rate by BM^{0.67} (W g^{-0.67}).

Respiratory capacity of permeabilized muscle fibres

Mice were killed by cervical dislocation. The triceps of the right front leg were then rapidly dissected and cut longitudinally to visualize the different types of fibre present in the skeletal muscle: red fibres (oxidative) towards the inside and white fibres (glycolytic) towards the outside. In order to obtain a mixture that was fairly representative of skeletal muscle, a muscle sample was transversely cut and placed in ice-cold isolation buffer (BIOPS containing 2.77 mmol l⁻¹ Ca-EGTA, 7.23 mmol l⁻¹ EGTA, 20 mmol l⁻¹ imidazole, 20 mmol l⁻¹ taurine, 50 mmol l⁻¹ K-MES, 0.5 mmol l⁻¹ DTT, 6.56 mmol l⁻¹ MgCl₂, 5.77 mmol l⁻¹ ATP and 15 mmol l⁻¹ phosphocreatine, pH 7.2).

Skeletal muscle fibres were permeabilized in BIOPS solution supplemented with saponin (50 µg ml⁻¹) according to a standard protocol (Pesta and Gnaiger, 2012). Permeabilized fibres were weighed and their respiration was monitored with a high-resolution respirometer (Oxygraph-2k, Oroboros Instruments, Innsbruck, Austria) in a hyper-oxygenated respiratory buffer maintained at 37°C (110 mmol l⁻¹ sucrose, 0.5 mmol l⁻¹ EGTA, 3 mmol l⁻¹ MgCl₂, 60 mmol l⁻¹ potassium lactobionate, 20 mmol l⁻¹ taurine, 10 mmol l⁻¹ KH₂PO₄, 1 g l⁻¹ fatty acid-free bovine serum albumin and 20 mmol l⁻¹ Hepes, pH 7.1), allowing a range of respirations maximized between 200 and 400 µmol l⁻¹ oxygen.

A mixture of respiratory substrates (5 mmol l⁻¹ pyruvate, 2.5 mmol l⁻¹ malate and 5 mmol l⁻¹ succinate) was added to obtain the basal respiration (state 2). The maximal fully uncoupled respiration (state 3_{unc}) was initiated by addition of 2 µmol l⁻¹ carbonyl cyanide *p*-tri-fluoromethoxy-phenylhydrazone (FCCP), in the presence of oligomycin (2 µg ml⁻¹), an inhibitor of ATP synthase. The integrity of the permeabilized fibres was checked by measuring oxygen consumption in the presence of 10 µmol l⁻¹ cytochrome *c*.

Mitochondrial isolation

All hindleg skeletal muscles and livers were rapidly removed, weighed and freshly used to assess mitochondrial bioenergetics. Skeletal muscles were cut up finely, homogenized with a Potter Elvehjem homogenizer (five passages) and then treated with protease (1 mg g⁻¹ muscle wet mass) for 5 min in an ice-cold buffer (100 mmol l⁻¹ sucrose, 50 mmol l⁻¹ KCl, 5 mmol l⁻¹ EDTA and 50 mmol l⁻¹ Tris-base, pH 7.4). The muscle mixture was diluted 1:2 in an isolation buffer and centrifuged at 1000 *g* for 10 min, and the resulting supernatant was centrifuged at 8700 *g* for

10 min. The pellet was resuspended in isolation buffer and centrifuged at 1000 *g* for 10 min to remove any cellular debris contaminating the mitochondrial suspensions. The supernatant was filtered through cheesecloth and centrifuged at 8700 *g* for 10 min to pellet the mitochondria. Liver mitochondria were isolated at 4°C as described by Salin and co-workers (2010) in ice-cold isolation buffer containing 250 mmol l⁻¹ sucrose, 1 mmol l⁻¹ EGTA and 20 mmol l⁻¹ Tris base, pH 7.3 (Salin et al., 2010). Protein content of the mitochondrial suspension was determined using the Biuret method with bovine serum albumin as standard.

Oxidative capacity and oxidative phosphorylation efficiency of mitochondria

Measurements of mitochondrial respiration were carried out in a glass cell fitted with a Clark electrode (Rank Brothers Ltd, Bottisham, UK) containing respiratory buffer maintained at 37°C (120 mmol l⁻¹ KCl, 5 mmol l⁻¹ KH₂PO₄, 3 mmol l⁻¹ Hepes, 2 mmol l⁻¹ MgCl₂, 1 mmol l⁻¹ EGTA and 0.3% w/v fatty acid-free bovine serum albumin, pH 7.4). Liver and muscle mitochondria were energized with a mixture of pyruvate (5 mmol l⁻¹), malate (2.5 mmol l⁻¹) and succinate (5 mmol l⁻¹). ATP synthase was inhibited by addition of oligomycin (2 µg ml⁻¹) to obtain non-phosphorylating respiration (state 4_{oligo}). Then, FCCP (2 µmol l⁻¹) was injected to obtain the maximal fully uncoupled respiration rate (state 3_{unc}). Respiratory control ratio (RCR), estimated as the state 3_{unc}/state 4_{oligo} ratio, was used as an indication of mitochondrial integrity.

Oxidative phosphorylation efficiency of liver and muscle mitochondria was determined at 37°C in a respiratory buffer supplemented with 20 mmol l⁻¹ glucose and 1.6 U ml⁻¹ hexokinase, with a mixture of respiratory substrates (5 mmol l⁻¹ pyruvate, 2.5 mmol l⁻¹ malate, 5 mmol l⁻¹ succinate). Different steady-state rates of phosphorylation were obtained by the addition of ADP at 20, 100 and 500 µmol l⁻¹. Oxygen consumption in the presence of 500 µmol l⁻¹ ADP corresponds to the maximal phosphorylating oxygen consumption (state 3_{ADP}). The rate of phosphorylating respiration was recorded for 2–3 min, then 100 µl of mitochondrial suspension was collected every 30 s for muscle mitochondria or every 1 min for liver mitochondria, and immediately quenched in 100 µl of ice-cold perchloric acid solution (10% HClO₄, 25 mmol l⁻¹ EDTA). Samples were centrifuged at 4°C and 20,000 *g* for 5 min (Sigma Laborzentrifugen, Osterode am Harz, Germany). Then, 180 µl of supernatant was neutralized with a solution containing 2 mol l⁻¹ KOH and 0.3 mol l⁻¹ Mops, and centrifuged at 4°C and 20,000 *g* for 5 min. Finally, glucose 6-phosphate content of the resulting supernatant was spectrophotometrically measured at 340 nm (BioTek Instruments SAS, Colmar, France) in an assay medium (7.5 mmol l⁻¹ MgCl₂, 3.75 mmol l⁻¹ EDTA and 50 mmol l⁻¹ triethanolamine-HCl, pH 7.4 at room temperature) supplemented with 0.5 mmol l⁻¹ NAD and 0.5 U glucose 6-phosphate dehydrogenase. The same experiments were done in the presence of oligomycin (2 µg ml⁻¹) to check that ATP synthesis was specific to the mitochondrial ATP synthase.

Statistical analyses

Non-parametric one-factor ANOVA (Kruskal–Wallis) followed by *post hoc* Conover tests were used to analyse body mass differences between species, respiratory capacity of permeabilized muscle fibres and mitochondrial oxygen consumption rate. Liver mass or relative liver mass (% of body mass) and body mass were transformed by the common logarithm (log₁₀), and the allometric

relationship between these variables was analysed with the linear model (lm) and the *post hoc* method for general linear hypotheses (Tukey method), with log₁₀BM and species as fixed factors, as well as the interaction between them. After transforming RMR, AMR and body mass by the common logarithm, allometric relationships between these variables were examined with the linear mixed-effect model (lme), with log₁₀BM and activity state as fixed factors, and individual as random factor. Non-phosphorylating and maximal phosphorylating mitochondrial oxygen consumption of the three mice was juxtaposed on allometric relationships published by Mélanie et al. (2019) and Cook's distances were estimated to

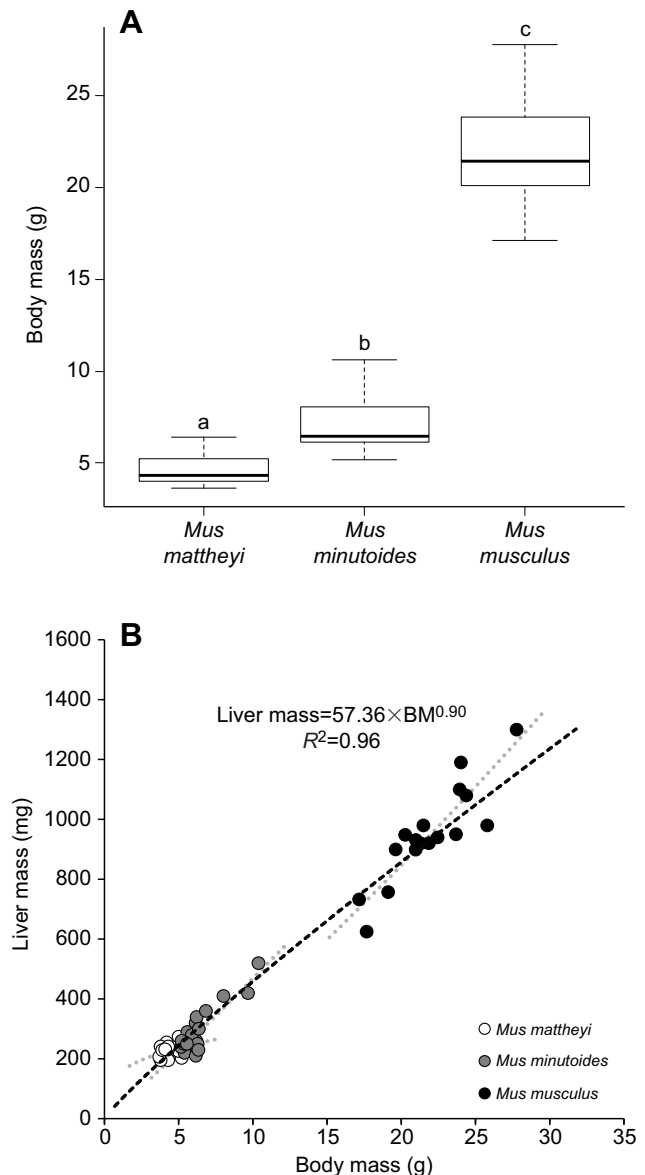


Fig. 1. Body mass and variation of liver mass with body mass for the three mouse species. (A) Mean \pm s.e.m. body mass for *Mus mattheyi* ($n=25$), *Mus minutooides* ($n=30$) and *Mus musculus* ($n=24$). Lowercase letters indicate significant differences between species ($P < 0.001$). (B) Liver mass (shown for each individual) co-varies positively with body mass (black dashed line, $P < 0.001$). Liver mass does not co-vary with body mass (BM) equivalently for *M. mattheyi* ($152.19 \times \text{BM}^{0.28}$) compared with *M. minutooides* ($39.96 \times \text{BM}^{1.07}$) and *M. musculus* ($22.67 \times \text{BM}^{1.21}$) because of an interaction between body mass and species factors (grey dotted line, $P < 0.01$).

highlight whether one species could be defined as an outlier. The allometric relationship between ATP synthesis and oxygen consumption was statistically analysed by lme followed by the *post hoc* method for general linear hypothesis with oxygen consumption and species as fixed factors, and individual as random factor. The interaction between oxygen consumption and species factors was also considered. After \log_{10} transformation of oxygen consumption, the relationship between mitochondrial coupling efficiency (ATP/O) and oxygen consumption was analysed with lme followed by a *post hoc* method for general linear model with $\log_{10}(\text{oxygen consumption})$ and species as fixed factors, and individual as a random factor. For all these allometric relationships, normality and homoscedasticity criteria for model residues were checked by the Shapiro–Wilk normality test coupled to the Plot Diagnostics for a lm object. Statistical analyses were done using a risk factor of 0.05 with R (<http://www.R-project.org/>) and the packages ‘stats’, ‘PMCMR’, ‘multcomp’, ‘nlme’, ‘mvtnorm’, ‘survival’, ‘TH.data’ and ‘MASS’. Data are generally presented as means \pm s.e.m., excepted for liver mass and whole-animal mass-specific oxygen consumption, where data for all tested individuals are presented.

RESULTS

All results of the statistical analyses carried out in this study are available in Table S1.

Body and liver mass

Body mass of the three species was significantly different, allowing an allometrical approach to the data ($P<0.001$; Fig. 1A): 4.69 ± 0.17 g (ranging from 3.6 to 6.4 g; $n=25$) for *M. mattheyi*, 7.12 ± 0.30 g (ranging from 5.2 to 10.6 g; $n=30$) for *M. minutoides* and 21.84 ± 0.55 g (ranging from 17.1 to 27.8 g; $n=24$) for *M. musculus* (means \pm s.e.m.). Liver mass is presented as a function of body mass in Fig. 1B. Liver mass rose 4.1-fold when body mass increased 5-fold ($P<0.001$). However, the interaction between body mass and species highlights that liver mass did not vary in the same way for *M. mattheyi* compared with the other two species ($P<0.01$). In this extremely small mammal, the body mass variation did not lead to a great liver mass variation compared with the other two species. Consequently, relative liver mass (as a percentage of body mass) co-varied negatively with body mass ($P<0.001$) and *M. mattheyi* had 1.2-fold higher relative liver mass than *M. musculus* (data not shown).

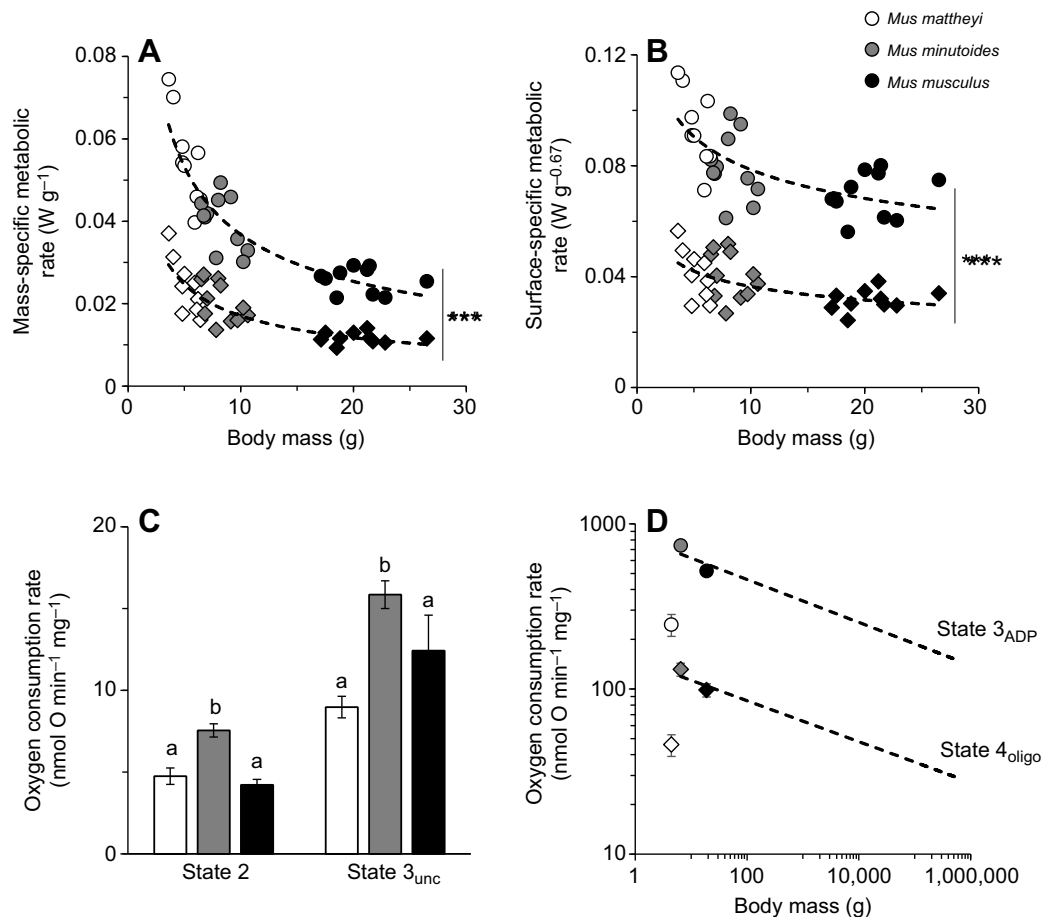


Fig. 2. Mass-specific metabolic rate at the whole-animal, cellular and subcellular level for the three mouse species. (A,B) Mass- and surface-specific whole-animal metabolic rate during rest (diamonds; $0.059\times\text{BM}^{-0.54}$, $R^2=0.75$ and $0.059\times\text{BM}^{-0.21}$, $R^2=0.85$, respectively) and activity (circles; $0.126\times\text{BM}^{-0.53}$, $R^2=0.31$ and $0.126\times\text{BM}^{-0.20}$, $R^2=0.45$, respectively) as a function of body mass. Data for each individual are presented. Resting and active metabolic rate co-vary negatively with body mass ($P<0.001$). Asterisks indicate a significant increase in metabolic rate with activity ($***P<0.001$). (C) Oxygen consumption rate of permeabilized muscle fibres at non-phosphorylating (state 2) and maximal uncoupled states (state 3_{unc}). Data are means \pm s.e.m. for *M. mattheyi* ($n=15$), *M. minutoides* ($n=18$) and *M. musculus* ($n=5$). Lowercase letters indicate significant differences between species ($P<0.001$). (D) Allometric relationship (dashed black lines) between basal (oligomycin; oxygen flux, $J_{\text{O}}=150\times\text{BM}^{-0.12}$, $R^2=0.91$) and maximal (ADP 500 $\mu\text{mol l}^{-1}$; $J_{\text{O}}=834\times\text{BM}^{-0.13}$, $R^2=0.82$) mitochondrial oxygen consumption and body mass from Mélanie et al. (2019), with the three species of the present study. Data are means \pm s.e.m. for *M. mattheyi* ($n=6$), *M. minutoides* ($n=6$) and *M. musculus* ($n=7$). Cook's distances for *M. mattheyi* were 1.25 and 0.96 for basal and maximal states, respectively.

Energy expenditure of animals and respiratory capacity of muscle fibres and mitochondria

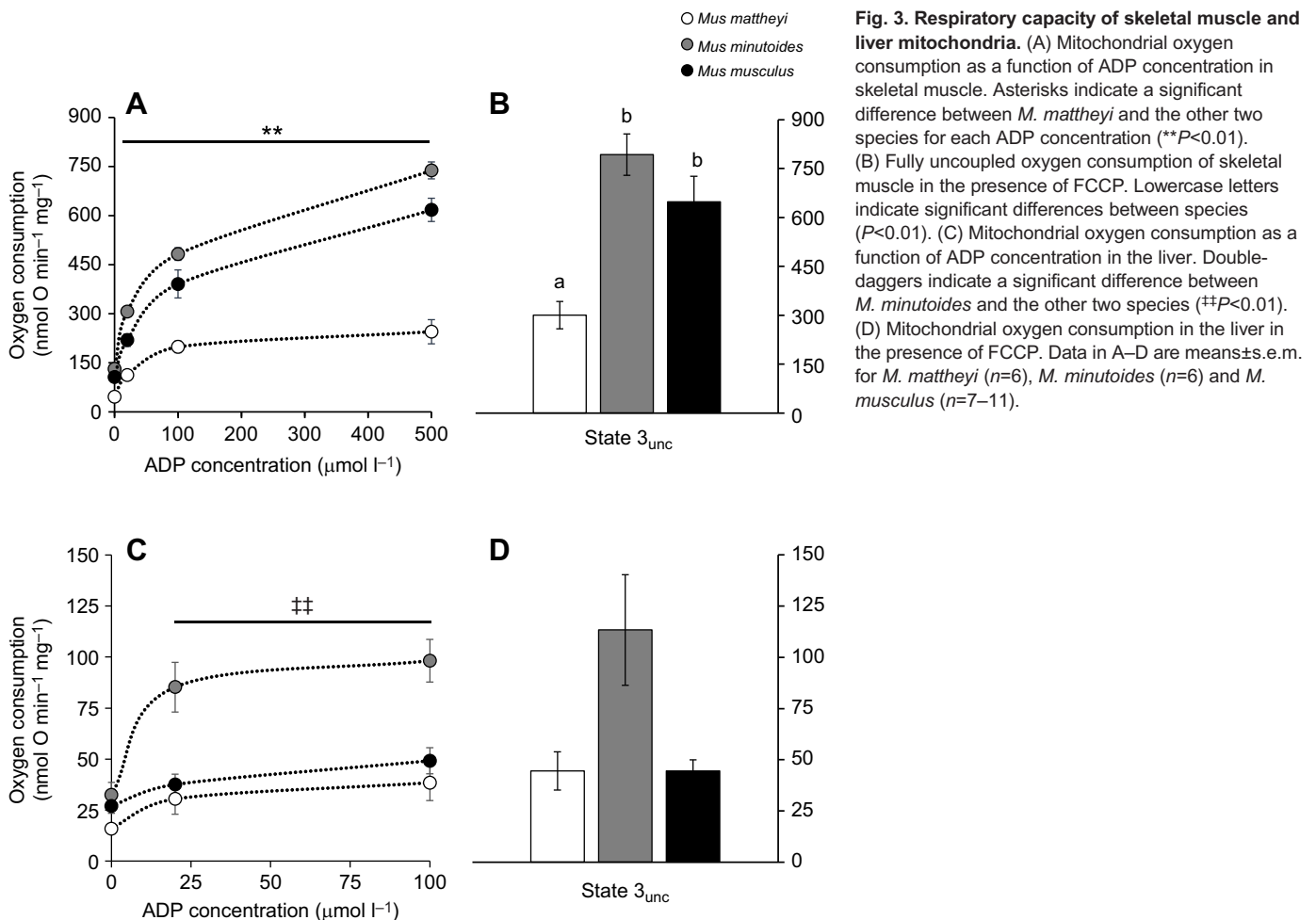
Mass- and surface-specific metabolic rate at rest (RMR) and in the active state (AMR) was obtained during the day and night, respectively, and is presented as a function of body mass (Fig. 2A,B). Metabolic rate rose significantly at night ($P<0.001$) and, irrespective of animal activity level, mass- and surface-specific metabolic rate declined 2.1- and 1.4-fold when body mass increased 4-fold ($P<0.001$).

The respiratory activity of permeabilized muscle fibres presented in Fig. 2C shows that permeabilized fibres of *M. mattheyi* and *M. musculus* consumed on average 1.6-fold less oxygen than those of *M. minutoides* ($P<0.001$ and $P<0.05$ for basal respiratory and fully uncoupled states, respectively). Basal non-phosphorylating (state 4_{oligo}) and maximal phosphorylating (state 3_{ADP}) oxygen consumption rates of muscle isolated mitochondria are reported in Fig. 2D. When mitochondrial data for the three mice species were juxtaposed to the allometric relationships published by Mélanie et al. (2019), Cook's distances for *M. mattheyi* were equal to 1.25 and 0.96 for non-phosphorylating and maximal phosphorylating oxygen consumption rate, respectively, and were on average at least 12-fold higher compared with values for the other two species. Accordingly, mitochondrial metabolism of *M. mattheyi* was significantly lower than that expected from allometric relationships in mammals (Mélanie et al., 2019).

Respiratory capacity and oxidative phosphorylation efficiency of isolated mitochondria

In skeletal muscle (Fig. 3A,B), *M. mattheyi* had significantly lower mitochondrial oxygen consumption rates than the other two species irrespective of energetic activity ($P<0.01$), i.e. irrespective of ADP concentration. The maximal activity of the electron transport system, i.e. the fully uncoupled state measured in the presence of FCCP (state 3_{unc}), was also significantly lower in *M. mattheyi* than in *M. minutoides* and *M. musculus* (Fig. 3B). On the whole, *M. mattheyi* consumed on average 2.5-fold less oxygen than the two other species. RCR values (*M. mattheyi* RCR=8.2±0.8, *M. minutoides* RCR=5.9±0.5, *M. musculus* RCR=6.2±0.4) were not significantly different between species ($K_2=5.56$, $P=0.06$). In liver (Fig. 3C), *M. mattheyi* and *M. musculus* consumed 2.4-fold less oxygen than *M. minutoides* regardless of ADP concentration ($P<0.01$). The maximal fully uncoupled state tended to give the same information, but data did not reach statistical significance ($P=0.058$; Fig. 3D). RCR value was higher ($K_2=8.17$, $P=0.02$) in *M. minutoides* than in *M. musculus*, and not different from that obtained in *M. mattheyi* (*M. mattheyi* RCR=3.2±0.2, *M. minutoides* RCR=4.2±0.4, *M. musculus* RCR=2.5±0.3).

Mitochondrial oxidative phosphorylation efficiency of liver and skeletal muscle is shown in Fig. 4. ATP synthesis rate increased linearly with oxygen consumption in skeletal muscle and liver mitochondria ($P<0.001$). In skeletal muscle mitochondria, maximal ATP synthesis and oxygen consumption flux were reduced 2.9-fold in *M. mattheyi* compared with *M. minutoides* ($P<0.01$; Fig. 4A).



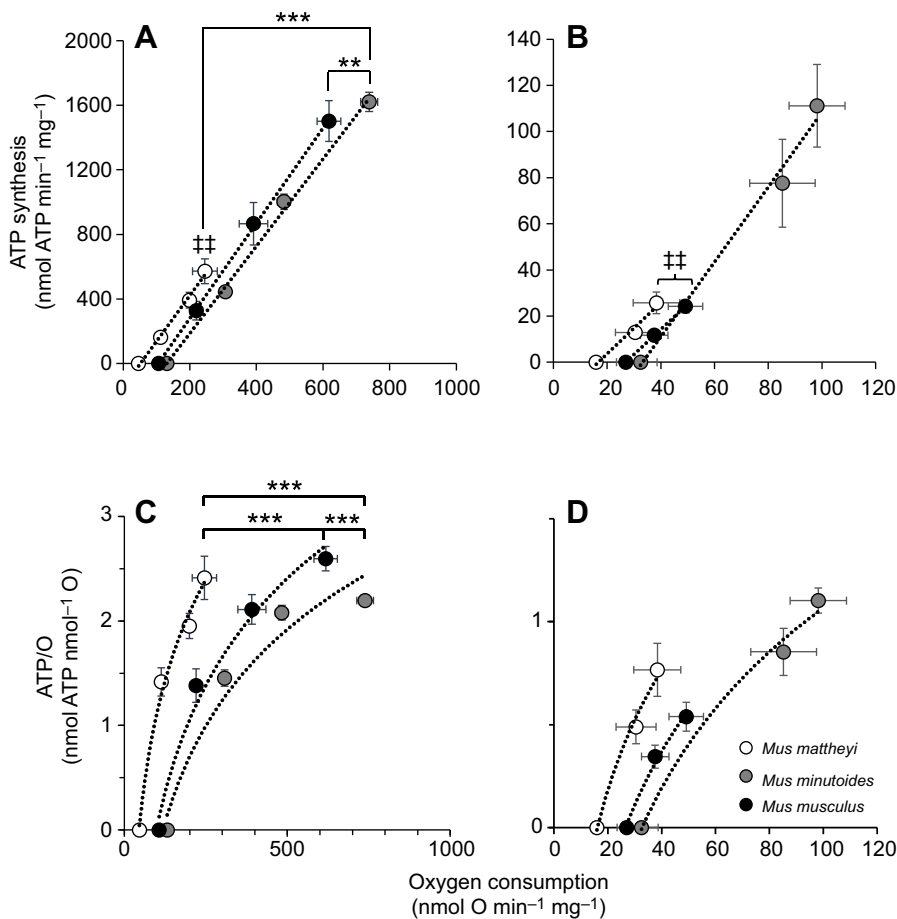


Fig. 4. Mitochondrial oxidative phosphorylation efficiency in skeletal muscle and liver for the three mouse species. (A) ATP synthesis as a function of oxygen consumption for skeletal muscle mitochondria ($P < 0.001$). Asterisks indicate that the linear relationship is shifted for, respectively, *M. musculus* and *M. mattheyi* compared with *M. minutoides* ($Z_2 = 3.43$, $**P < 0.01$ and $Z_2 = -4.52$, $***P < 0.001$). Double-daggers indicate that maximal mitochondrial flux was lower in *M. mattheyi* than in *M. minutoides* ($##P < 0.01$). (B) ATP synthesis as a function of oxygen consumption for liver mitochondria ($P < 0.001$). Double-daggers indicate that maximal mitochondrial flux was higher in *M. minutoides* than in the other two species ($##P < 0.01$). (C) ATP/O as a function of oxygen consumption for skeletal muscle mitochondria. Asterisks indicate a significant difference ($***P < 0.001$) for *M. mattheyi* versus *M. musculus* ($Z_2 = -7.66$), *M. mattheyi* versus *M. minutoides* ($Z_2 = -9.61$) and *M. musculus* versus *M. minutoides* ($Z_2 = 3.72$). (D) ATP/O as a function of oxygen consumption for liver mitochondria. Data in A–D are means \pm s.e.m. for *M. mattheyi* ($n = 6$), *M. minutoides* ($n = 6$) and *M. musculus* ($n = 7-11$).

Moreover, linear curves for *M. mattheyi* and *M. musculus* were significantly shifted to the left compared with that for *M. minutoides* ($P < 0.001$), even after considering the interaction between oxygen consumption and species ($P < 0.01$). As a result, *M. mattheyi* consumed on average 2.8-fold less oxygen than *M. minutoides* to synthesize the same amount of ATP. Accordingly, although the three species may reach the same maximal mitochondrial coupling efficiency (ATP/O), *M. mattheyi* consumed less oxygen than the other two species for a given ATP/O ($P < 0.001$), as illustrated in Fig. 4C. For instance, for maximal ATP/O, *M. mattheyi* consumed 245 ± 37 nmol O min⁻¹ mg⁻¹ protein compared with 739 ± 26 and 618 ± 36 nmol O min⁻¹ mg⁻¹ for *M. minutoides* and *M. musculus*, respectively. In liver, maximal ATP synthesis and oxygen consumption were respectively on average 4-fold and 2-fold lower in *M. mattheyi* and *M. musculus* compared with *M. minutoides* ($P < 0.01$; Fig. 4B). Although the results resemble those of the skeletal muscle, linear curves for *M. musculus* and *M. mattheyi* were not significantly shifted to the left. The strong interaction between oxygen and species factors ($P < 0.001$) masked a species effect ($P < 0.01$). Consequently, considering the interaction, the results of the *post hoc* test indicated that the three species consumed the same amount of oxygen for a given ATP/O (Fig. 4D).

DISCUSSION

The fundamental conclusion of this comparative study is that the negative relationship between mass-specific metabolism and body mass obtained at the whole-animal level is not necessarily maintained at the cellular and mitochondrial levels for the three species chosen here. Mass-specific metabolic rate of mice rises

when body mass declines (Fig. 2A), and the few grams of difference between the extremely small African pygmy mice *M. mattheyi* (~4.7 g) and *M. minutoides* (~7.1 g) lead to a marked increase of this metabolism, regardless of their activity (RMR and AMR), as predicted by the allometric trends (Pearson, 1948; Hayssen and Lacy, 1985; Glazier, 2005). Even if differences in heat loss between species were considered, the negative relationship between surface-specific metabolism and body mass was conserved (Fig. 2B). At cellular and sub-cellular levels, *M. minutoides* followed the allometric pattern, with higher respiration rates in both permeabilized fibres and isolated mitochondria, together with lower efficiency at least in skeletal muscle mitochondria compared with values for *M. musculus*. These findings are congruent with those of previous studies (Krebs, 1950; von Bertalanffy and Pitozynski, 1951; Porter and Brand, 1995a; Couture and Hulbert, 1995; Porter, 2001; Mélanie et al., 2019) and partly explain the high metabolic rate at the whole-animal level. In contrast, results concerning *M. mattheyi* were overall counter-intuitive with a strong dissonance between metabolism at the whole-animal and cellular levels. Indeed, this extremely small mouse exhibited high mass- and surface-specific metabolic rates at the whole-animal scale associated with surprisingly low respiratory capacity at cellular and mitochondrial levels (high Cook's distance compared with other mammalian species). Whether such a depression of cellular metabolic activity also occurs in other highly metabolically active tissues such as the heart and kidney remains unknown and deserves further investigation. The hypothesis of a mitochondrial adaptation, by which extremely small species would avoid a very strong mitochondrial proton leakage and associated energy wastage in

order to maintain their cellular energy homeostasis, is thus verified in two tissues of *M. mattheyi*.

This discrepancy in the allometric relationship from whole-animal to cellular levels might also be explained by differences in relative mass of metabolically active tissues and/or mitochondrial content of these tissues, which are two other phenotypic traits influencing whole-body metabolism. Liver mass varied positively with body mass, as observed in the literature (Holliday et al., 1967; Calder, 1996). However, this variation with body mass was not equivalent in each of the species studied, with *M. mattheyi* having relatively small variance in liver mass, irrespective of body mass, leading to a much greater relative liver mass in smaller individuals compared with larger ones. Previous publications showed that the mass of other metabolically active tissues co-varies allometrically with body mass according to a scaling exponent less than 1 (e.g. liver, kidney, heart and brain but excluding skeletal muscle, which exhibits an allometric exponent equal to 1 in mammals), suggesting a higher proportion of these tissues in small species compared with larger ones (Schmidt-Nielsen, 1984; Else and Hulbert, 1985a,b). Applying the exponent published in Else and Hulbert (1985b) to the present mouse species, *M. mattheyi* would have 1% and 3% more of these total active tissues compared with *M. minutoides* and *M. musculus*, respectively. We could not exclude that the high metabolic activity and heat production in *M. mattheyi* may also be associated with a larger amount of brown adipose tissue involved in heat generation (Himms-Hagen, 1990). In line with this idea, artificial selection for large and small body mass in mice leads to differences in thermoregulatory performance, with small mice having a higher proportion of brown adipose tissue compared with larger ones (Lynch and Roberts, 1984). The difference in the proportion of metabolically active tissues could become even more important if the mass of these tissues has not evolved equivalently within each species, as in the present data for the liver. This last point highlights the importance of studying the covariation of mass of other metabolically active tissues with body mass. Finally, mitochondrial content or volume in liver, kidney, heart and skeletal muscles has previously been shown to be negatively correlated with body mass (Smith, 1956; Else and Hulbert, 1985b; Porter and Brand, 1995b). In the present study, the mitochondrial content of skeletal muscle, as estimated by the ratio between fully uncoupled respiratory activity (state 3_{unc}) measured in fibres (Fig. 2B) and mitochondria (Fig. 3A), suggests that *M. mattheyi* had approximately 70% (~34 mg g⁻¹ of muscle) higher content than *M. minutoides* and *M. musculus* (~20 mg g⁻¹ of tissue). Although this difference remains to be carefully measured, a close estimation and similar conclusion can be reached using the allometry of mammalian cytochrome *c* content in skeletal muscle (Drabkin, 1950). All these data suggest that *M. mattheyi* may generally have more mitochondria and metabolically active tissues than the other two species, but further studies are needed to validate these suggestions.

Furthermore, *M. mattheyi* exhibited higher mitochondrial coupling efficiency in their skeletal muscles. The improvement of coupling efficiency might have some benefits for very small mammals. In particular, maintaining ATP production at a lower oxygen consumption rate would alleviate the constraint of the very high energy supply, normally expected in small organisms to sustain their very high metabolic rate. As far as *M. mattheyi* is concerned, one can hypothesize that the improvement of muscle efficiency might reduce the metabolic cost of locomotion and thus increase their foraging performance (Conley, 2016; Bourguignon et al., 2017). However, the improvement of muscle mitochondrial

efficiency in *M. mattheyi* is also associated with a lower maximal activity of proton leak, suggesting lower heat production at rest. Hence, having large numbers of skeletal mitochondria that are less leaky but more coupled may require *M. mattheyi* to allocate energy from daily activity to thermoregulation, using muscular work as a heat generator in order to maintain body temperature (Humphries and Careau, 2011). If so, such a hypothesis would predict a higher daily activity in *M. mattheyi* than in other *Mus* species. The increased mitochondrial efficiency in the very small mice *M. mattheyi* was not found in *M. minutoides*, whose average body mass was 7 g. This might suggest a limit of such mitochondrial ‘innovation’ which would occur only for extremely low-mass species. Whether other extremely small mammals like the Etruscan shrew (*Suncus etruscus*, ~2 g) or the pygmy jerboa (*Salpingotulus michaelis*, ~4 g) have also adapted their mitochondrial bioenergetics profile is currently unknown, but it clearly deserves further investigation.

In conclusion, small species sustain important heat loss dissipation and raise their mass- or surface-specific metabolism to stay warm. This general trend has been often observed, regardless of biological scale. However, bioenergetics profile changes due to physiological constraints imposed by an extremely small mass can lead to discrepancies between whole-animal, cellular and mitochondrial scales. Indeed, the mitochondria of *M. mattheyi* were as coupled as those of *M. musculus*, which suggests that this extremely small mammal has adapted its bioenergetics profile to ensure ATP homeostasis for cellular activity and other individual performances. These data provide key elements in understanding the physiology of extremely small endotherms but raise a number of questions to explore.

Acknowledgements

We warmly thank the rodent breeding facility of Montpellier University (CECEMA) and Marie Challe for her help in maintaining the colonies of pygmy mice, as well as Angeline Clair, Laetitia Averty and Julie Ulmann of the EcoAquatron (FR3728), who ensured the breeding and maintenance of the *M. musculus* colony. We also thank Stephan and Sylvie Basinski for reviewing the English in the manuscript.

Competing interests

The authors declare no competing or financial interests.

Author contributions

Conceptualization: D.R., Y.V.; Methodology: D.R., Y.V.; Validation: D.R., Y.V.; Formal analysis: M.B., C.R., C.D., D.R.; Investigation: M.B., C.R., C.D., D.R.; Writing - original draft: M.B.; Writing - review & editing: C.R., C.D., F.V., S.R., D.R., Y.V.

Funding

This work was supported by the French Government [to M.B., PhD grants 2016–2019], by the Fédération de Recherche BioEnviS – FR3728 of University Claude-Bernard Lyon 1.

Supplementary information

Supplementary information available online at <http://jeb.biologists.org/lookup/doi/10.1242/jeb.215558.supplemental>

References

- Blackburn, T. M. and Gaston, K. J. (1994). Animal body size distributions: patterns, mechanisms and implications. *Trends Ecol. Evol.* **9**, 471–474. doi:10.1016/0169-5347(94)90311-5
- Boback, S. M. and Guyer, C. (2003). Empirical evidence for an optimal body size in snakes. *Evol. Int. J.* **57**, 345–351. doi:10.1111/j.0014-3820.2003.tb00268.x
- Bourguignon, A., Rameau, A., Toullec, G., Romestaing, C. and Roussel, D. (2017). Increased mitochondrial energy efficiency in skeletal muscle after long-term fasting: its relevance to animal performance. *J. Exp. Biol.* **220**, 2445–2451. doi:10.1242/jeb.159087
- Brand, M. D., Turner, N., Ocloo, A., Else, P. L. and Hulbert, A. J. (2003). Proton conductance and fatty acyl composition of liver mitochondria correlates with body mass in birds. *Biochem. J.* **376**, 741–748. doi:10.1042/bj20030984
- Britton-Davidian, J., Robinson, T. J. and Veyrunes, F. (2012). Systematics and evolution of the African pygmy mice, subgenus *Nannomys*: a review. *Acta Oecol.* **42**, 41–49. doi:10.1016/j.actao.2012.01.001

- Brown, J. H.** (1995). *Macroecology*, 2nd edn.: University of Chicago Press.
- Caldar, W. A.** (1996). *Size, Function, and Life History*: Courier Corporation.
- Conley, K. E.** (2016). Mitochondria to motion: optimizing oxidative phosphorylation to improve exercise performance. *J. Exp. Biol.* **219**, 243-249. doi:10.1242/jeb.126623
- Couture, P. and Hulbert, A. J.** (1995). Relationship between body mass, tissue metabolic rate, and sodium pump activity in mammalian liver and kidney. *Am. J. Physiol.* **268**, R641-R650. doi:10.1152/ajpregu.1995.268.3.r641
- Divakaruni, A. S. and Brand, M. D.** (2011). The regulation and physiology of mitochondrial proton leak. *Physiology* **26**, 192-205. doi:10.1152/physiol.00046.2010
- Drabkin, D. L.** (1950). The distribution of the chromoproteins, hemoglobin, myoglobin, and cytochrome c, in the tissues of different species, and the relationship of the total content of each chromoprotein to body mass. *J. Biol. Chem.* **182**, 317-334.
- Eise, P. L. and Hulbert, A. J.** (1985a). An allometric comparison of the mitochondria of mammalian and reptilian tissues: the implications for the evolution of endothermy. *J. Comp. Physiol. B Biochem. Syst. Environ. Physiol.* **156**, 3-11. doi:10.1007/BF00692920
- Eise, P. L. and Hulbert, A. J.** (1985b). Mammals: an allometric study of metabolism at tissue and mitochondrial level. *Am. J. Physiol. Regul. Integr. Comp. Physiol.* **248**, R415-R421. doi:10.1152/ajpregu.1985.248.4.R415
- Falconer, D. S.** (1973). Replicated selection for body weight in mice. *Genet. Res.* **22**, 291-321. doi:10.1017/S0016672300013094
- Gardezi, T. and da Silva, J.** (1999). Diversity in relation to body size in mammals: a comparative study. *Am. Nat.* **153**, 110-123. doi:10.1086/303150
- Glazier, D. S.** (2005). Beyond the '3/4-power law': variation in the intra- and interspecific scaling of metabolic rate in animals. *Biol. Rev. Camb. Philos. Soc.* **80**, 611-662. doi:10.1017/S1464793105006834
- Hayssen, V. and Lacy, R. C.** (1985). Basal metabolic rates in mammals: taxonomic differences in the allometry of BMR and body mass. *Comp. Biochem. Physiol.* **81**, 741-754. doi:10.1016/0300-9629(85)90904-1
- Heldmaier, G.** (1989). Seasonal acclimatization of energy requirements in mammals: functional significance of body weight control, hypothermia, torpor and hibernation. In *Energy Transformations in Cells and Organisms* (ed. W. Wieser and E. Gnaiger), pp. 129-139. Thieme.
- Hillesheim, E. and Stearns, S. C.** (1992). Correlated responses in life-history traits to artificial selection for body weight in *Drosophila melanogaster*. *Evolution* **46**, 745-752. doi:10.1111/j.1558-5646.1992.tb02080.x
- Himms-Hagen, J.** (1990). Brown adipose tissue thermogenesis: interdisciplinary studies. *FASEB J.* **4**, 2890-2898. doi:10.1096/fasebj.4.11.2199286
- Holliday, M. A., Potter, D., Jarrah, A. and Bearg, S.** (1967). The relation of metabolic rate to body weight and organ size. *Pediatr. Res.* **1**, 185-195. doi:10.1203/00006450-196705000-00005
- Hoole, C., Czenze, Z. J., Bennett, N. C. and McKechnie, A. E.** (2019). Thermal physiology of three sympatric small mammals from southern Africa. *J. Zool.* **307**, 28-35. doi:10.1111/jzo.12613
- Humphries, M. M. and Careau, V.** (2011). Heat for nothing or activity for free? Evidence and implications of activity-thermoregulatory heat substitution. *Integr. Comp. Biol.* **51**, 419-431. doi:10.1093/icb/ucr059
- Keijer, J., Li, M. and Speakman, J. R.** (2019). What is the best housing temperature to translate mouse experiments to humans? *Mol. Metab.* **25**, 168-176. doi:10.1016/j.molmet.2019.04.001
- Krebs, H. A.** (1950). Body size and tissue respiration. *Biochim. Biophys. Acta* **4**, 249-269. doi:10.1016/0006-3002(50)90032-1
- Lusk, G.** (1924). Animal calorimetry twenty-four paper. Analysis of the oxidation of mixtures of carbohydrate and fat. *J. Biol. Chem.* **59**, 41-42.
- Lynch, C. B. and Roberts, R. C.** (1984). Aspects of temperature regulation in mice selected for large and small size. *Genet. Res.* **43**, 299-306. doi:10.1017/S0016672300026082
- Malerba, M. E., White, C. R. and Marshall, D. J.** (2018). Eco-energetic consequences of evolutionary shifts in body size. *Ecol. Lett.* **21**, 54-62. doi:10.1111/ele.12870
- McMahon, T. and Bonner, J. T.** (1983). *On Size and Life*, 1st edn: Scientific American Library.
- Mélanie, B., Caroline, R., Yann, V. and Damien, R.** (2019). Allometry of mitochondrial efficiency is set by metabolic intensity. *Proc. R. Soc. B* **286**, 20191693. doi:10.1098/rspb.2019.1693
- Pearson, O. P.** (1947). The rate of metabolism of some small mammals. *Ecology* **28**, 127-145. doi:10.2307/1930947
- Pearson, O. P.** (1948). Metabolism of small mammals, with remarks on the lower limit of mammalian size. *Science* **108**, 44-44. doi:10.1126/science.108.2793.44
- Pesta, D. and Gnaiger, E.** (2012). High-resolution respirometry: OXPHOS protocols for human cells and permeabilized fibers from small biopsies of human muscle. *Methods Mol.* **810**, 25-58. doi:10.1007/978-1-61779-382-0_3
- Peters, R. H.** (1983). *The Ecological Implications of Body Size* by Robert Henry Peters: Cambridge Core.
- Polymeropoulos, E. T., Heldmaier, G., Frappell, P. B., McAllan, B. M., Withers, K. W., Klingenspor, M., White, C. R. and Jastroch, M.** (2011). Phylogenetic differences of mammalian basal metabolic rate are not explained by mitochondrial basal proton leak. *Proc. R. Soc. B* **279**, 185-193. doi:10.1098/rspb.2011.0881
- Porter, R. K.** (2001). Allometry of mammalian cellular oxygen consumption. *Cell. Mol. Life Sci.* **58**, 815-822. doi:10.1007/PL000090902
- Porter, R. K. and Brand, M. D.** (1993). Body mass dependence of H⁺ leak in mitochondria and its relevance to metabolic rate. *Nature* **362**, 628-630. doi:10.1038/362628a0
- Porter, R. K. and Brand, M. D.** (1995a). Cellular oxygen consumption depends on body mass. *Am. J. Physiol. Regul. Integr. Comp. Physiol.* **269**, R226-R228. doi:10.1152/ajpregu.1995.269.1.R226
- Porter, R. K. and Brand, M. D.** (1995b). Causes of differences in respiration rate of hepatocytes from mammals of different body mass. *Am. J. Physiol. Regul. Integr. Comp. Physiol.* **269**, R1213-R1224. doi:10.1152/ajpregu.1995.269.5.r1213
- Porter, R. K., Hulbert, A. J. and Brand, M. D.** (1996). Allometry of mitochondrial proton leak: influence of membrane surface area and fatty acid composition. *Am. J. Physiol.* **271**, 1550-1560. doi:10.1152/ajpregu.1996.271.6.R1550
- Reynolds, P. S.** (1997). Phylogenetic analysis of surface areas of mammals. *J. mamm.* **78**, 859-868. doi:10.2307/1382944
- Roberts, R. C.** (1966). The limits to artificial selection for body weight in the mouse II. The genetic nature of the limits. *Genet. Res.* **8**, 361-375. doi:10.1017/S0016672300010211
- Roberts, R. C.** (1981). The growth of mice selected for large and small size in relation to food intake and the efficiency of conversion. *Genet. Res.* **38**, 9-24. doi:10.1017/S0016672300020371
- Rolfe, D. F. and Brand, M. D.** (1996). Contribution of mitochondrial proton leak to skeletal muscle respiration and to standard metabolic rate. *Am. J. Physiol.* **271**, C1380-C1389. doi:10.1152/ajpcell.1996.271.4.C1380
- Rolfe, D. F. S. and Brand, M. D.** (1997). The physiological significance of mitochondrial proton leak in animal cells and tissues. *Biosci. Rep.* **17**, 9-16. doi:10.1023/A:1027327015957
- Rolfe, D. F. and Brown, G. C.** (1997). Cellular energy utilization and molecular origin of standard metabolic rate in mammals. *Physiol. Rev.* **77**, 731-758. doi:10.1152/physrev.1997.77.3.731
- Rolfe, D. F. S., Newman, J. M. B., Buckingham, J. A., Clark, M. G. and Brand, M. D.** (1999). Contribution of mitochondrial proton leak to respiration rate in working skeletal muscle and liver and to SMR. *Am. J. Physiol.* **276**, C692-C699. doi:10.1152/ajpcell.1999.276.3.C692
- Salin, K., Teulier, L., Rey, B., Rouanet, J.-L., Voituron, Y., Duchamp, C. and Roussel, D.** (2010). Tissue variation of mitochondrial oxidative phosphorylation efficiency in cold-acclimated ducklings. *Acta Biochim. Pol.* **57**, 409-412. doi:10.18388/abp.2010_2426
- Schmidt-Nielsen, K.** (1984). *Scaling: Why is Animal Size so Important?*: Cambridge University Press.
- Smith, R. E.** (1956). Quantitative relations between liver mitochondria metabolism and total body weight in mammals. *Ann. N. Y. Acad. Sci.* **62**, 405-421. doi:10.1111/j.1749-6632.1956.tb35360.x
- Terrien, J., Perret, M. and Aujard, F.** (2011). Behavioral thermoregulation in mammals: a review. *Front. Biosci. (Landmark edition)* **16**, 1428-1444. doi:10.2741/3797
- Veyrunes, F., Britton-Davidian, J., Robinson, T. J., Calvet, E., Denys, C. and Chevret, P.** (2005). Molecular phylogeny of the African pygmy mice, subgenus *Nannomys* (Rodentia, Murinae, Mus): implications for chromosomal evolution. *Mol. Phylogenet. Evol.* **36**, 358-369. doi:10.1016/j.ympev.2005.02.011
- von Bertalanffy, L. and Pitozynski, W. J.** (1951). Tissue respiration and body size. *Science* **114**, 307. doi:10.1126/science.114.2960.307

Table S1 : Results of statistical analyses for the different parameters studied

Tested variable	Test	Effect	DF	Test value	p-value	Effective (<i>M. mattheyi</i> , <i>M. minutoides</i> , <i>M. musculus</i>)
Body mass						
	Kruskal-Wallis	Species	2	64.491	< 0.001	25, 30, 24
Liver mass						
	Linear model	log(body mass)	1	1689.770	< 0.001	
		species	2	4.163	0.022	16, 19, 17
		log(body mass):species	2	6.174	0.004	
Relative liver mass						
	Linear model	log(body mass)	1	19.637	< 0.001	
		species	2	4.163	0.022	16, 19, 17
		log(body mass) :species	2	6.174	0.004	
Mass-specific metabolic rate – log(metabolic rate) as a function of log(body mass)						

	Linear model	log(body mass)	1, 26	159.265	< 0.001	9, 11, 5
		Activation state	1, 29	573.457	< 0.001	
Surface-specific metabolic rate – log(metabolic rate) as a function of log(body mass)						
	Linear model	log(body mass)	1, 26	25.299	< 0.001	9, 11, 5
		Activation state	1, 29	573.457	< 0.001	
Respiratory capacities of permeabilized muscular fibers						
State 2	Kruskal-Wallis	species	2	16,990	< 0.001	15, 18, 10
State 3 _{unc}	Kruskal-Wallis	species	2	19,602	< 0.001	15, 18, 10
Respiratory capacities of skeletal muscle mitochondria						
0 μM (Oligomycine)	Kruskal-Wallis	species	2	15.975	< 0.001	6, 6, 7
20 μM ADP	Kruskal-Wallis	species	2	15.583	< 0.001	6, 6, 7
100 μM ADP	Kruskal-Wallis	species	2	11.991	0.002	6, 6, 7
500 μM ADP	Kruskal-Wallis	species	2	15.219	< 0.001	6, 6, 7
State 3 _{unc}	Kruskal-Wallis	species	2	12.492	0.002	6, 6, 7
Respiratory capacities of liver mitochondria						
0 μM (Oligomycine)	Kruskal-Wallis	Species	2	7.050	0.029	6, 6, 11

20 μ M ADP	Kruskal-Wallis	Species	2	11.219	0.004	6, 6, 11
100 μ M ADP	Kruskal-Wallis	Species	2	11.097	0.004	6, 6, 11
State 3 _{unc}	Kruskal-Wallis	species	2	5.672	0.059	6, 6, 11

Maximal ATP syntheses for skeletal muscle and liver mitochondria

Skeletal muscle	Kruskal-Wallis	Species	2	12.952	0.002	6, 6, 7
Liver	Kruskal-Wallis	Species	2	12.68	0.002	6, 6, 11

Mitochondrial efficiency of skeletal muscle

ATP vs. oxygen	Linear mixed-effect model	oxygen	1, 66	4574.604	< 0.001	6, 6, 7
		species	2, 20	22.763	< 0.001	
		Oxygen:species	2, 66	5.686	0.005	
ATP/O vs. log(oxygen)	Linear mixed-effect model	Log(oxygen)	1, 68	485.130	< 0.001	6, 6, 7
		species	2, 20	48.351	< 0.001	

Mitochondrial efficiency of liver

ATP vs. oxygen	Linear mixed-effect model	oxygen	1, 41	485.305	< 0.001	
		species	2, 19	8.152	0.003	6, 6, 11
		Oxygen:species	2, 41	40.562	< 0.001	
ATP/O vs. log(oxygen)	Linear mixed-effect model	Log(oxygen)	1, 43	109.219	< 0.001	
		species	2, 19	2.271	0.088	6, 6, 11